

On the strength of microalloyed steels - An interpretive review

C. I. Garcia, M. Hua, K. Cho, A. J. DeArdo

In the mid-1950s, hot rolled carbon steels exhibited high carbon contents, coarse ferrite-pearlite microstructures, and yield strengths near 300 MPa. Their ductility, toughness and weldability were poor. Today, a half-century later, hot rolled steels can exhibit microstructures consisting of mixtures of ferrite, bainite and martensite in various proportions. These structures are very fine and can show yield strengths over 900 MPa, with acceptable levels of ductility, toughness and weldability.

This advancement was made possible by the combination of improved steelmaking, microalloying technology and better rolling and cooling practices. The purpose of this paper is to chronicle some of the remarkable progress in steel alloy and process design that has resulted in this impressive.

KEYWORDS:

Accelerated cooling, direct quenching, EBSD-IQ, HSLA steel, strengthening, thermomechanical processing, transformation

INTRODUCTION: MICROALLOYING AND STRENGTH

The year 1980 represents a benchmark in the strength of MA steels. From the early days of the 1960s to approximately 1980, the steels being microalloyed were low hardenability steels with ferrite-pearlite (F-P) microstructures and yield strengths up to about 420 MPa (60 Ksi). These were the steels that were used to develop the principles and interrelationships of microalloying, controlled rolling and air cooling. They were characterized by relatively higher carbon contents and moderate Mn levels, and exhibited ferrite-pearlite (F-P) microstructures after air cooling (1).

Around 1980, both the pipeline and the automotive industries desired strengths in excess of the 420 MPa that could be readily supplied with fine grained F-P steels. Clearly higher strength microstructures were required. The obvious choices were the lower temperature transformation products: matrices comprised of non-polygonal ferrite, acicular ferrite, the bainites and martensite, either as monoliths or as mixtures. To achieve these microstructures, the combination of higher hardenability and high cooling rates was required. Furthermore, much additional research was needed to reach the required goals consistently and with uniform results.

From the processing side, the solution to this dilemma was using water cooling after hot rolling. This was accomplished in the mid-1980s for plate processing by interrupted accelerated cooling (IAC) and interrupted direct quenching (IDQ) in plate mills. Runout table water spray cooling to the coiling temperature in hot strip mills had been in practice since the 1960s, but not as

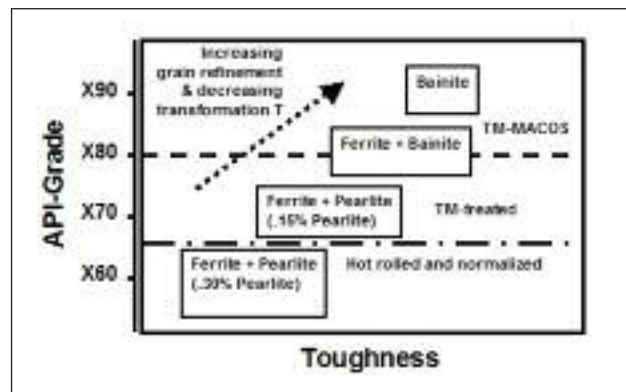


FIG. 1 Evolution of plate steel for large diameter pipeline: microstructure and mechanical properties. (2)

Evoluzione dell'acciaio per lamiera destinato a condutture di grande diametro: proprietà microstrutturali e meccaniche. (2)

a microstructural control tool for increasing strength. This was because of the higher carbon contents of the steels of that era. The benefits of faster rates of cooling and lower coiling temperatures were exploited for achieving higher strengths later with steels of lower carbon contents.

Figure 1 shows schematically how the microstructure and properties of plate steels changed over time with advances in alloy design and processing (2).

It is obvious from Figure 1, that the accelerated cooling after rolling was largely responsible for the very high strengths attainable, practically independent of composition. With suitable cooling practices, yield strengths in excess of 690 MPa (X100) can be achieved in low carbon steels containing less than 2 Wt% Mn and with C. E. and Pcm values near 0.5 and 0.2, respectively (3, 4). One central question is what is the role of the MAE in obtaining these strength levels? Let's begin with the early steels (pre-1980), where air cooling of plate and high coiling temperatures of strip were used. As noted above, these were the F-P steels with strengths up to about 420 MPa (X60) for gauges up to 18mm (0.7 inches). The most obvious contributor to strength was grain refinement, as was clearly shown by quantitative optical micro-

C. Issac Garcia, Mingjian Hua,
Kengun Cho, A. J. DeArdo

BAMPRI (The Basic Metals Processing Research Institute)
Department of Mechanical Engineering and Materials Science - University of Pittsburgh, Pittsburgh, Pennsylvania 15261, USA

Anthony DeArdo
Finland Distinguished Professor,
Department of Mechanical Engineering
University of Oulu, P.O. Box 4200 (Linnanmaa),
FIN-90014, Finland

Paper presented at the 3rd International Conference Thermomechanical Processing of Steels, Padova, 10-12 september 2008, organized by AIM

	NbC	NbN	VC	VN
Lattice Parameter, a_0 , nm	4.4702	4.39	4.16	4.29
[100]ppt // [100] γ	25.22	22.98	16.53	20.17
[010]ppt // [010] γ	25.22	22.98	16.53	20.17
[001]ppt // [001] γ	25.22	22.98	16.53	20.17
[100]ppt // [100] α	55.95	53.15	45.13	49.67
[011]ppt // [010] α	10.26	8.28	2.61	5.81
[0-11]ppt // [001] α	10.26	8.28	2.61	5.81

TAB. 1
Lattice mismatch for MX precipitates in austenite and ferrite, % Austenite: fcc, $a_0 = 0.35698$ nm; Ferrite: bcc, $a_0 = 0.28664$ nm.
Differenze dei parametri reticolari per precipitati MX nell' austenite e nella ferrite, % Austenite: fcc, $a_0 = 0.35698$ nm; Ferrite: bcc, $a_0 = 0.28664$ nm.

scopy. There is no doubt that the MAE was responsible for this contribution through its effect on austenite conditioning. Other contributions included solid solution strengthening by the Mn, Si, and others, including the MAE, when retained in solution. Equations have been published quantifying these effects, as well (5). The other contribution to strength claimed by researchers studying these early steels was precipitation hardening (6). The precipitates expected to strengthen ferrite, NbCN, VCN, TiC, TiN, all exhibit a NaCl crystal structure, and, as such, do not fit well in the ferrite lattice. The lattice mismatch for Nb and V precipitates in both austenite and ferrite are shown in Table 1 (7). This explains why the MA particles are always located on crystalline defects in either the austenite or ferrite (7). The misfit strains of several percent mean that the particles cannot be coherent. The combination of incoherency with the ferrite and the NaCl structure means that the particles must cause strengthening by the Orowan-Ashby mechanism, Eq. 1 (8-10).

$$\Delta FSI_{(ppt)} = ((M \cdot K + G \cdot b) / (\sigma \cdot \lambda))^{1/2} \cdot (1.2 [(\sigma \cdot \lambda)^{1/2} / \sigma] - [\ln(\lambda / 2b)])$$

$$\text{or } \Delta FSI_{(ppt)} = 6982 [(\sigma \cdot \lambda)^{1/2} / \sigma] - [\ln(2\sigma b)] \quad (1)$$

This mechanism of strengthening for the Orowan process is by: (a) the energy required for dislocations to bow between particles, and (b) the energy required by the cross slipping of screw segments

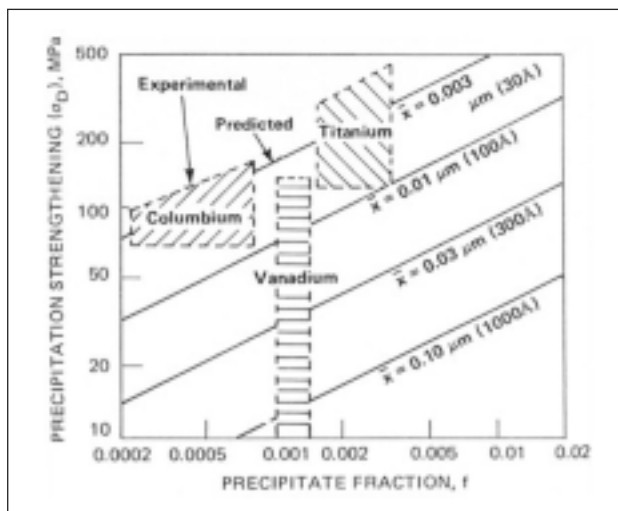


FIG. 2 *The dependence of precipitation strengthening on precipitate size (X) and fraction according to the Ashby-Orowan Model, compared with experimental observations for given microalloying additions. (10)*
Dipendenza dell' indurimento per precipitazione dalla dimensione (X) e dalla frazione in volume dei precipitati secondo il modello Ashby-Orowan, confrontata con osservazioni sperimentali a seguito di aggiunte mirate di microalliganti. (10)

or climb of edge dislocation segments in bypassing the particles (9). The predicted increase in YS caused by this mechanism depends on the amount or volume fraction of precipitate and the size of the particles. This is shown for particles in ferrite in Figure 2 by Gladman for several precipitation systems (10).

The data of Figure 2 must be used with caution, however. First, the volume fraction or amount used in the calculation is that actually consumed in forming the particles. The amount lost to the austenite in rolling and the amount remaining in solid solution do not contribute to the strength shown in Figure 2 and must be subtracted from the total. Second, the precipitates participating are those actually present in the steel, and, therefore, need time to form in the ferrite. An early example of the slow kinetics for this precipitation was shown by Honeycombe and Sakuma (11, 12), Figure 3, and later confirmed by Thillou, et al. (13). Third, claims of precipitation hardening and the application of Figure 2 should be independently verified by thin foil TEM. Fourth, the mere presence of fine particles in ferrite does not guarantee precipitation hardening. The distribution must conform to the Orowan-Ashby model to justify claims of a certain level of strengthening. Finally, it must be recognized that isothermal laboratory experiments do not necessarily predict the behavior of continuously cooled commercial steels, even when the compositions are similar.

Plots of the Orowan-Ashby equation as viewed from what must be observed in thin foil TEM are shown in Figure 4 (14,15). These plots show what precipitate distributions must be present, viz. measured, to claim 10, 50 and 100 MPa increments in YS caused by precipitation hardening. Superimposed are reason-

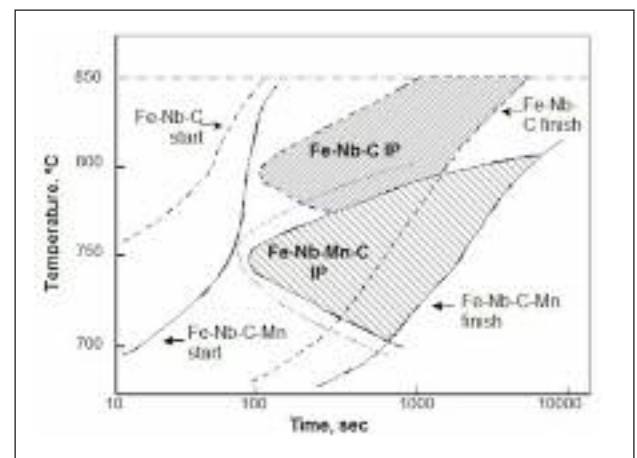


FIG. 3 *Schematic TTT curves for Fe-0.036Nb-0.09C and Fe-0.036Nb-0.09C-1.07Mn alloys. Interphase precipitation (IP) occurs in certain shaded areas.*
Curve TTT schematiche per leghe Fe-0.036Nb-0.09C e Fe-0.036Nb-0.09C-1.07Mn. La precipitazione interfase (IP) si verifica entro le aree tratteggiate.

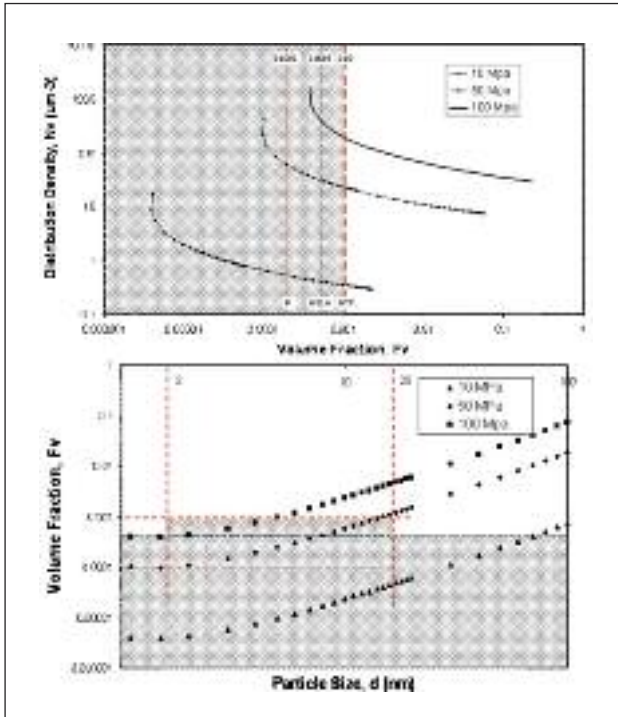


FIG. 4 Particle dispersion characteristics for precipitate strengthening according to Orowan-Ashby theory. (14,15)

Caratteristiche della dispersione delle particelle all'origine dell' indurimento per precipitazione secondo la teoria Orowan-Ashby. (14, 15)



FIG. 5 Interphase precipitation of NbCN in ferrite in steel containing .09%C - .07%Nb. Specimen reheated at 1250°C, rolled at 1000°C, and air cooled to RT. (19)

Precipitazione interfase di NbCN nella ferrite di un in acciaio contenente .09%C - .07%Nb. Campioni riscaldati a 1250°C e raffreddati in aria fino a temperatura ambiente. (19)

ble levels of both particle size and volume fractions. The predictions of Figures 4 and 5 are fully consistent with the data of Figure 2. The Gladman diagram shown in Figure 2 represents the maximum strengthening increments that can be expected when conditions for precipitation are ideal, i.e. full precipitation of available components. Again, the abscissa in Figure 2 is the volume fraction actually formed, not what is predicted from the bulk composition. In commercially processed hot rolled steels, it is extremely rare that increments caused by precipitation hardening exceed 50-80 MPa (16). This magnitude is comparable to

that found by solution hardening and bake hardening or strain aging (16), and is nowhere near what can be found by dislocation or substructure strengthening of ferrite (16-18).

In discussions of precipitation hardening in MA steels, the cooling path from the finish rolling temperature is critical to the formation of strengthening particles (7, 11, 12). While air cooling at 1°C/sec from 750-600°C in 150 sec. might be slow enough to form strengthening precipitates, Figure 5 (19), water spray cooling through the temperature range 750-600°C at 10-50°C/sec is probably much too fast to form effective particle distributions in rolled and cooled steels.

In summary, the major role of the MAE in strengthening the pre-1980 steels was mainly by grain refinement. To this was probably added some solid solution and dislocation strengthening. The contribution by precipitation hardening is not zero, but has been probably over estimated. This was pointed out in several early studies (20, 21).

The strength of these steels can be understood by Equation (2), the expanded Hall-Petch equation.

$$YS_{obs} = YS_{P-N} + \Delta YS_{SS} + \Delta YS_{texture} + \Delta YS_{disl} + \Delta YS_{pptn} + K_y d^{-1/2} \quad (2)$$

where YS_{obs} is the observed yield strength; YS_{P-N} , YS_{SS} , $YS_{texture}$, YS_{disl} , YS_{pptn} are the stress increments caused by lattice friction (Peierls-Nabarro), solid solution, texture, dislocations, and precipitation; and $K_y d^{-1/2}$ represents the contribution by the ferrite grain size.

For the F-P steels of the 1970s, the dominant contribution to strength was $K_y d^{-1/2}$, with much smaller contributions from YS_{SS} , YS_{disl} , and YS_{pptn} .

MODERN STEELS

As was noted earlier, in the 1980s there was a large emphasis on increasing the strength from the 420 MPa (API-X60) level to over 490 (API X-70). On the process side, this challenge was met by lowering the transformation temperature of the austenite during the cooling after hot rolling. On plate mills, this was accomplished by interrupted accelerated cooling (IAC) and later by interrupted direct quenching (IDQ). On strip mills it was achieved by increasing the cooling rate and lowering the coiling temperature. In plate rolling, controlled rolling followed by air cooling has been termed TMP, while controlled rolling followed by IAC or IDQ has been called TMCP in some quarters (22).

It is well known that accelerated cooling can increase the strength of F-P steels by reducing the ferrite grain size, as shown in numerous studies (20,23). What is less clear is that rapid cooling leading to refined polygonal ferrite also leads to higher ferrite grain center hardness, as shown by Morikawa and Hasegawa, Figure 6 (24).

The 0.15C-0.66Mn steel used in Figure 6 showed that the ferrite grain center hardness, viz., a volume not thought to be strongly influenced by grain boundaries or grain refinement, increased substantially with cooling rate from about 100Hv at 1°C/sec to near 140Hv at 100°C/sec. This increase was attributed to higher solute C and excess dislocations present in the rapidly cooled ferrite. No bainite was observed until cooling rates exceeded 25°C/sec. in this experiment. This extra strengthening was attributed to the combination of higher solute carbon levels trapped in rapidly cooled ferrite and to higher dislocation densities.

MULTI-PHASE MATRIX MICROSTRUCTURES

The equally important change with cooling rate involves the matrix microstructure. It is obvious from Figure 1 that the difference between the 420 and >490 MPa grades is the nature of

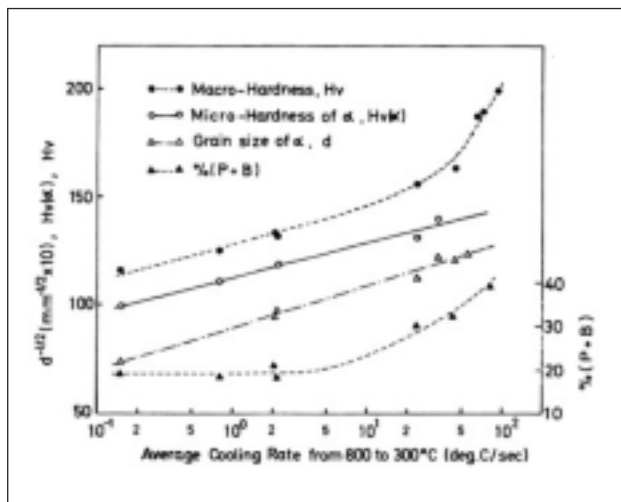


FIG. 6 Effect of cooling rate on strengthening factors of steel 1. (24)

Effetto della velocità di raffreddamento sui fattori di indurimento dell'acciaio 1. (24)

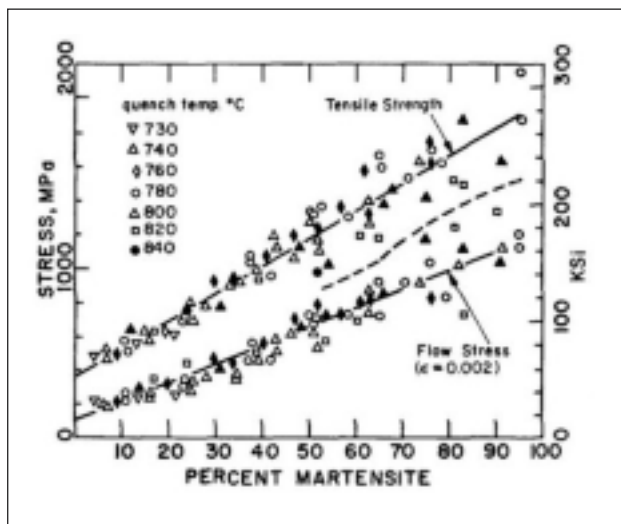


FIG. 7 The 0.2% flow stress and the tensile strength as a function of percent martensite for Fe-Mn-C alloys. (25)

Limite di snervamento allo 0,2% e carico di rottura in funzione della percentuale di martensite per le leghe Fe-Mn-C. (25)

the matrix (2). As noted earlier, the 420 MPa grade shows polygonal ferrite formed at high transformation temperatures, over perhaps 600°C. The matrix in higher strength steels shows mixtures of ferrite and bainite and/or martensite, in different proportions. In general, the higher the proportion of bainite and martensite, the higher the strength of the steel.

As the strength level increases, the steels change character from monolithic ferrite to complex mixtures starting with ferrite-bainite, ferrite-martensite, monolithic bainite, and finally monolithic martensite. With mixed microstructures, the steels appear to follow the Rule of Mixtures, as shown by Davies in Figure 7 for ferrite-martensite mixtures found in DP automotive steels (25). The influence of MAE on the transformation characteristics of controlled rolled and cooled steels can be profound, especially at higher rates of cooling. An example of this effect is shown in Figures 8-10 (7,26) for transformation start temperatures, resulting microstructures and final mechanical properties, respectively (7, 26).

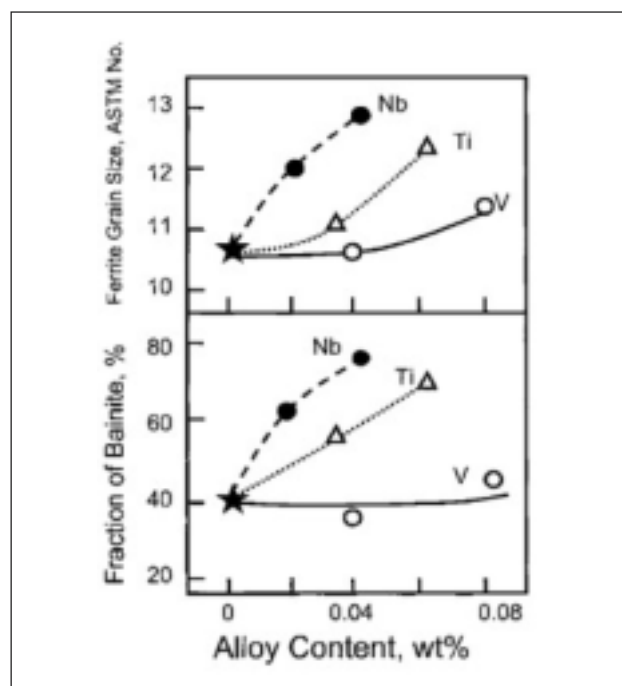


FIG. 9 Effects of Nb, V and Ti on volume fraction of bainite and ferrite grain size in accelerated cooled steels (7, 26).

Effetti di Nb, V e Ti sulla frazione in volume della diverse dimensioni dei grani di bainite e ferrite in acciai sottoposti a raffreddamento accelerato (7, 26)

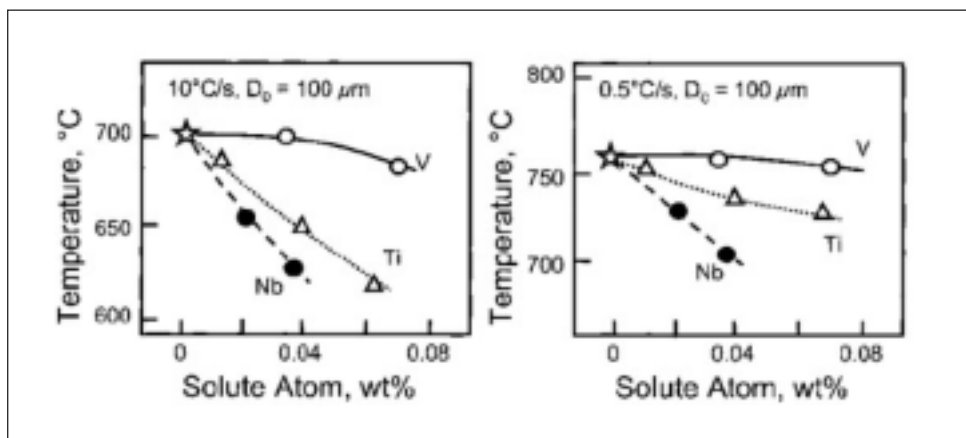
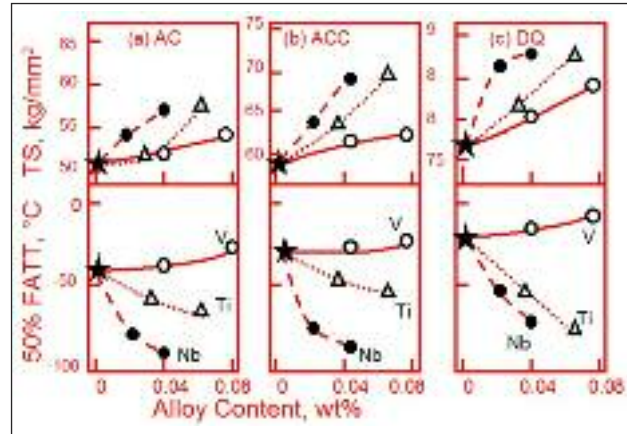


FIG. 8 Corrected A_{r3} temperatures of microalloyed steels with standard austenite grain size of 100 μ m (7, 26).

Temperature A_{r3} corrette per acciai microlegati con dimensione standard del grano austenitico (100 μ m) (7, 26).

FIG. 10 *Effects of addition of Nb, V and Ti on tensile strength and Charpy V 50% FATT of (1) air cooled, (2) accelerated cooled and (3) direct quenched steels after controlled rolling (7, 26).*

Effetti dell'aggiunta di Nb, V e Ti sulla resistenza a trazione e sulla 50% FATT Charpy V di acciai (1) raffreddati ad aria, (2) sottoposti a raffreddamento accelerato e (3) temprati direttamente dopo laminazione controllata (7, 26)



The positive synergy between the MAE and accelerated cooling is significant. Figure 10 reveals that the addition of 0.04 wt% Nb to the base steel adds about 10% to the strength after air cooling; accelerated cooling with Nb adds about 40% and DQ with Nb adds about 76%. Other examples show how the addition of Nb, Figure 11 or V, Figure 12, to a 0.07C - 1.55Mn - 0.018Ti reference steel has little effect on the final microstructure after air cooling but a large effect after accelerated cooling, especially on strength (27).

MONOLITHIC MICROSTRUCTURES

It is well-known that low carbon and ultra-low carbon bainitic and martensitic ferrite can exhibit remarkable properties. Yield strengths in excess of 850 MPa (X120) in 12-18mm plate and strip have been achieved in MA steels processed using TMCP (3, 4). Two obvious questions are: (i) what can cause the strength to essentially double from the early 350-420MPa grades to the newer 700-850MPa grades, and (ii) what is the role, if any, of the MAE?

It is well known that the strength of bainite and martensite is controlled mainly by the carbon content and the Bs or Ms temperature (28, 29), Figure 13. The data of Figure 13 were generated with ULCB plate steels with rich chemistries intended for heavy gauge applications (29).

Attempts have been made to relate the properties of bainite to its microstructure, but with limited success (30-32). With falling temperature and increasing strength, the sequence of upper bainite, granular bainite, then lower bainite is often observed. Although these microconstituents have different appearances in the OM, their real microstructure must be revealed by thin foil TEM. Since this is a very tedious and expensive proposition, little of this work has been done. What is clear from the available literature is that with falling Bs temperature, both the soluble carbon content and the dislocation density increase. This is why the strength increases with falling transformation temperatures. The main reason that the soluble carbon content increases with falling temperature can be related to the sloping upper ferrite solvus and T_0 lines on the Fe-Fe₃C phase diagram and the Hultgren extrapolation that exist in the absence of cementite (33, 34). They predict that in the absence of equilibrium, viz. presence of Fe₃C, higher cooling rates will lead to higher carbon contents with falling temperature. This, together with the large solution hardening capability of carbon and the concomitant increase in the dislocation density resulting from the combination of the volume change and the shear-type nature of the transformation will combine to result in higher

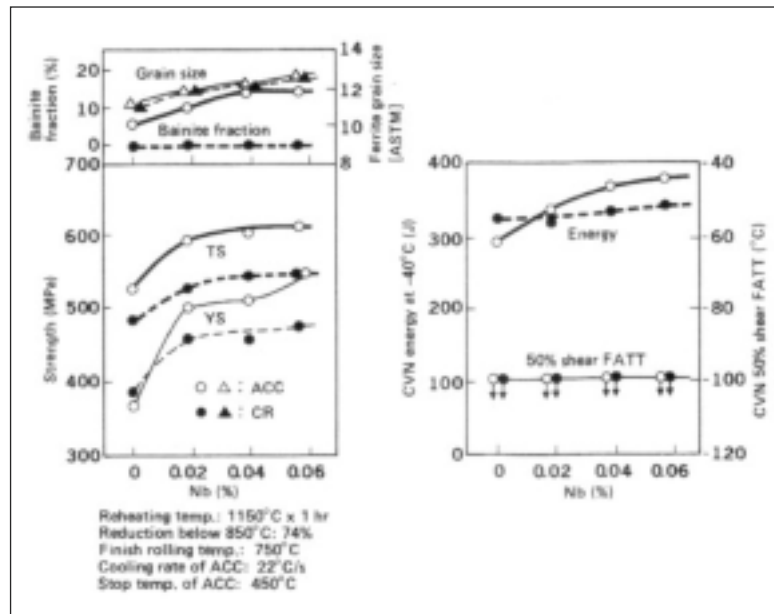


FIG. 11 *Effect of Nb content on properties of plate (27). CR denotes controlled rolling and air cooling; ACC denotes controlled rolling and accelerated cooling.*

Effetti del contenuto di Nb sulle proprietà dei laminati (27). CR indica laminazione controllata e raffreddamento ad aria; ACC indica laminazione controllata e raffreddamento accelerato.

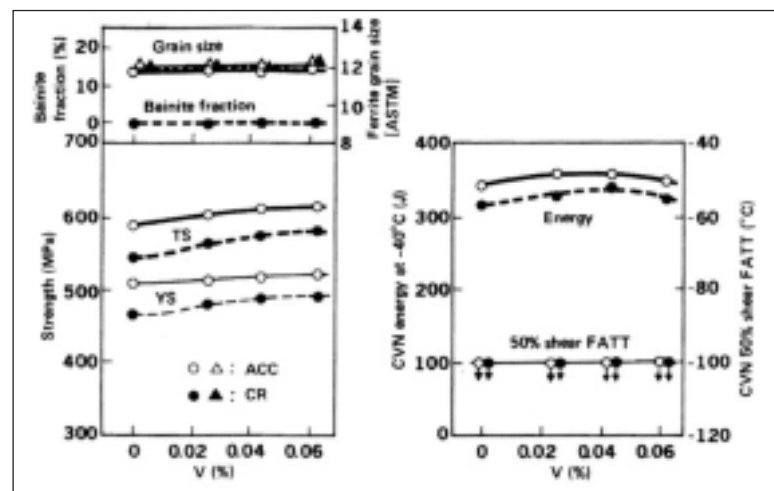


FIG. 12 *Effect of V content on properties of plate (27)*

Effetto del contenuto di V sulle proprietà dei laminati (27).

strengths with falling temperature.

One way to characterize the microstructure, one that avoids the confusion and complexity of labeling and characterizing the observed ultra-fine detail, is through the use of EBSD-IQ, a technique recently applied to microstructure assessment in advanced steels (35). In the EBSD-IQ technique, once the specimen surface and beam stability effects have been eliminated, the quality of the final diffraction peaks coming from the Kikuchi lines is measured, processed and quantified (35). Highly elastically distorted lattices yield low IQ peaks since the diffraction profile is smeared, not unlike line broadening due to elastic strain in x-ray diffraction (36). Near-perfect lattices yield high IQ peaks, because the peaks in the diffraction pattern are narrow and sharp. Since both solute elements, viz. C and N, and dislocations as well as precipitates might contribute to lattice strain, the EBSD-IQ approach to understanding the strength of bainite and martensite appears to be promising.

Recent work using the EBSD-IQ technique has shown that multi-phase microstructures can be characterized and quantified using this approach. In this technique, the EBSD-IQ data are first processed and then plotted using the Multi-Peak Software (35). The resulting plots show a spectrum of multiple peaks where the peak height is proportional to the volume fraction of that microconstituent and the location on the abscissa is related to the inverse of the lattice distortion. As noted above, this distortion is assumed to come from the combination of lattice strain caused by the dislocation density, solute content and particles.

Typical examples are shown for studies involving HSLA strip, Figures 14 and 15 (35,37, 38), DP steel, Figure 16 (35,39), TRIP-assisted steels (40), heat treated seamless pipe, Figure 17 (38) and bainitic plate steels, Figure 18 (41). It is clear that this technique can discern details of the final microstructure, including the components of multi-phase mixtures.

The first example of applying the EBSD-IQ technique to multi-phase microstructures is to an HSLA hot band structure with an optical microstructure as shown in Figure 14. Analyzing this complex microstructure using the EBSD-IQ approach resulted if

the multi-peak profile shown in Figure 15. Notice the several forms of ferrite present in the microstructure.

The next example is a DP steel where the amounts of ferrite and martensite were measured in three ways; by point counting, by image analysis and the third by EBSD-IQ. The IQ results are shown in Figure 16. The phase balance values determined with the three approaches fell within a few percent (35,39).

Another example is heat treated seamless pipe that shows a mixture of autotempered and untempered martensite after tempering. The EBSD-IQ analysis of this steel is shown in Figure 17 (38).

Finally, the EBSD-IQ approach has been applied to bainitic steel plates. The IQ analysis of this study revealed the multi-peak result shown in Figure 18 (41).

When considering the strength of the bainite or martensite, either as a monolithic matrix or as part of mixed microstructures, certain aspects must be considered. First, there are relatively few high angle boundaries present in the microstructure. Therefore Hall-Petch strengthening will not be important. Second, very little precipitation hardening can be expected in these rapidly cooled steels, at least in the as-cooled condition (42).

Hence, the strength of the bainite and/or martensite will be go-

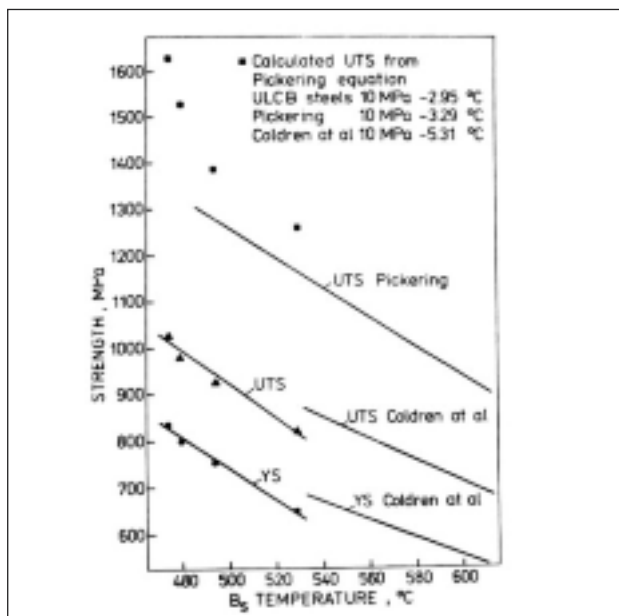


FIG. 13 Comparison of measured and calculated strength values for a given B_s temperature. (29)

Confronto dei valori di resistenza meccanica misurati e calcolati per una determinata temperatura B_s . (29)

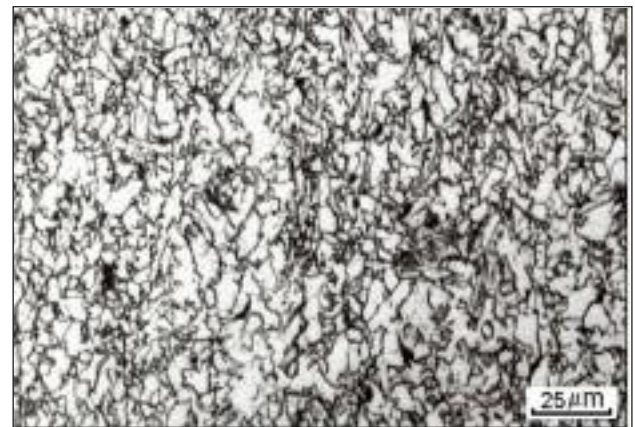


FIG. 14 Optical micrograph of a HSLA steel hot band. Etched with 2% Nital. (35,37)

Micrografia ottica di un nastro a caldo in acciaio HSLA. Attacco Nital 2%. (35, 37)

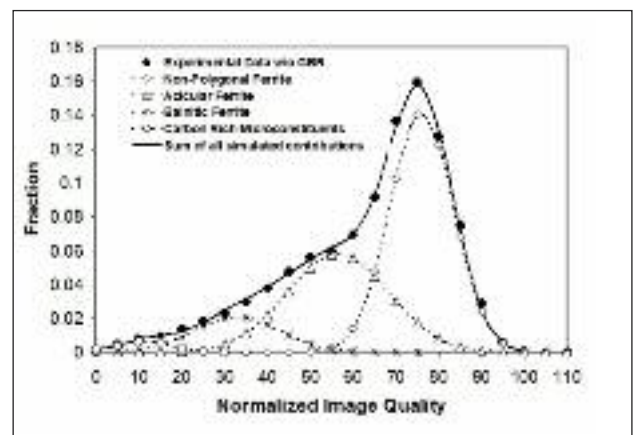


FIG. 15 The IQ analysis of the HSLA hot band microstructure shown in Figure 14 using the Multi-Peak model. (35,38)

Analisi IQ della microstruttura del nastro a caldo in acciaio HSLA mostrato in Fig. 14 mediante modello Multi-Peak (35, 38)

verned by the contributors to lattice distortion, viz. solutes, dislocations and their interaction. Early examples of these strong dislocation effects were shown by Smith and Honeycombe (17), Manganon and Heitmann (18), and Repas (43).

The influence of dislocation density or subgrain size on strength can be very much higher than those from solid solution and precipitation, where increments of 30-80 MPa are typical. Manganon and Heitmann have shown that substructure hardening of ferrite can easily exceed 200MPa, Figure 19 (18). This is a contribution that can also be expected in bainite and cannot be overlooked.

In summary, when the strength of bainite is considered through the lens of the expanded Hall-Petch equation, the contributions from YS_{disl} and YS_{ss} are probably most important and the contributions from high angle grain boundaries and precipitation are secondary.

CONCLUSIONS

It is no surprise that the microstructures of the 200-420 MPa YS steels of the 1960s and 1970s are very different from those of the >490 grades of today. It is rather amazing that the steels

have nearly doubled in strength while still maintaining adequate, if not superior levels of other important properties such as toughness, weldability, ductility, formability, etc. These improvements have been facilitated by evolutions of steelmaking, rolling and cooling practices. The details of the improvements have been chronicled and are largely understood. Perhaps the main message learned over the past 50 years, or so, is that microstructural improvement and optimization are often not a simple extrapolation of the old to the new. Sometimes we need a new box.

REFERENCES

1. Proc. Microalloying 75 (Washington, DC), Union Carbide Corp., New York, 1977.
2. M. K. Graff, H. G. Hillenbrand and P. A. Peters, "Accelerated Cooling of Plate for High-Strength Large Diameter Pipe," Accelerated Cooling of Steel, TMS-AIME, Warrendale, PA, USA, 1986, 165-180.
3. H. Asahi et al., "Development and Properties of Ultra High-strength UOE Pipeline," Proc. IPC 2004, International Pipeline Conference, Oct. 4-8, 2004, Calgary, Alberta, Canada, ASME 2004, paper # IPC04-0230.
4. D. Bai, L. Collins, F. Hamad, X. Chen, and R. Klein, "Microstructure and Mechanical Properties of High Strength Linepipe Steels,"

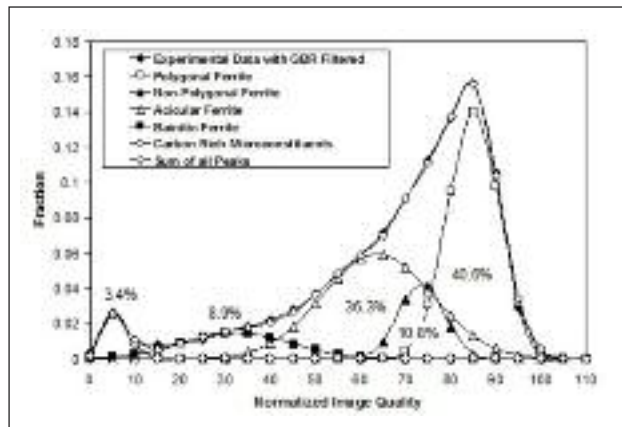


FIG. 16 IQ analysis of DP steel microstructure using multi-peak model. (35)

Analisi IQ di una microstruttura di acciaio DP mediante modello Multi-Peak (35)

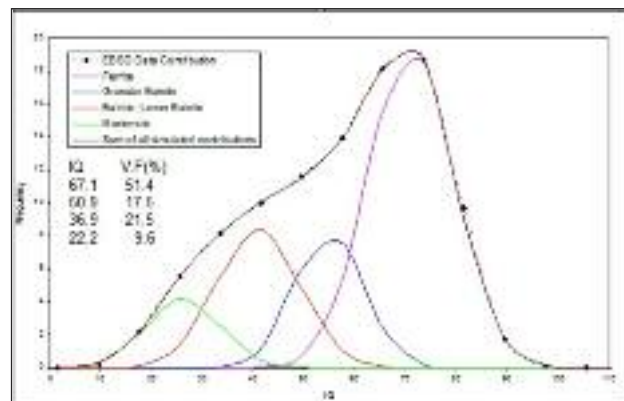


FIG. 18 EBSD IQ multi-peak analysis of a bainitic steel.

Analisi EBSD IQ multi-peak di un acciaio bainitico.

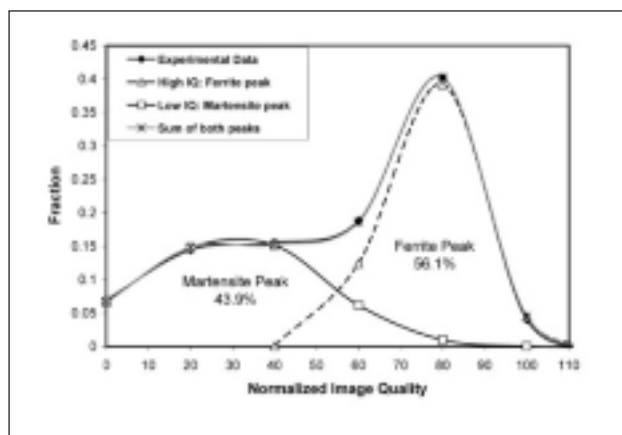


FIG. 17 The Image Quality (IQ) distribution analysis of the specimen cooled by 10°C/sec, A508 Gr4N steel.

Analisi di distribuzione con Image Quality (IQ) del provino di acciaio A508 Gr4N raffreddato a 10°C/s.

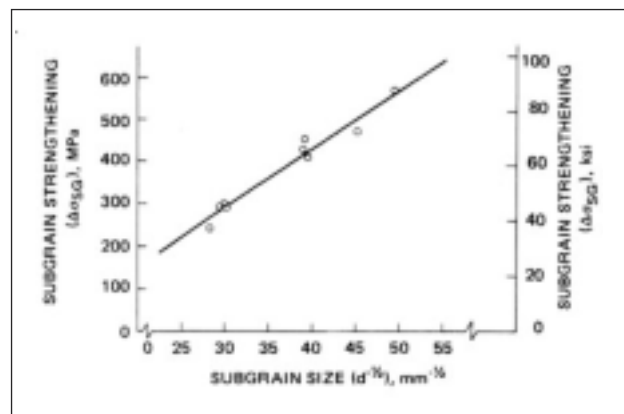


FIG. 19 Regression line between subgrain size (d) and its strengthening effect ($\Delta\sigma_{SC}$). Note that $d^{-1/2} = 30, 40$ and 50 is equivalent to approximately $1.1, 0.63$ and $0.4 \mu\text{m}$ cell size, respectively.

Linea di regressione fra dimensione del sottograno (d) e il suo effetto di indurimento ($\Delta\sigma_{SC}$). Notare che $d^{-1/2} = 30, 40$ e 50 è equivalente a una dimensione di cella rispettivamente di circa $1,1 - 0,63 - 0,4 \mu\text{m}$.

- MS&T07, 355-366.
5. H. Yada: "Prediction of Microstructural Changes and Mechanical Properties in Hot Strip Rolling," Accelerated Cooling of Rolled Steel, ed. by G. E. Ruddle and A. F. Crawley, Pergamon Press, New York (1988), 105.
 6. W. B. Morrison, Journal of the Iron and Steel Institute, 201, 317 (1963).
 7. A. J. DeArdo, "Niobium in Modern Steels," International Materials Reviews, Vol. 48, No. 6, (2003), pp.371-402.
 8. J. Friedel, Dislocations (Oxford: Pergamon Press, 1967).
 9. L. M. Brown, R. H. Cook, R. K. Ham, G. R. Purdy, Scripta Metallurgica, Vol. 7, (1973), 815-820.
 10. T. Gladman, D. Duliou and I. D. McIvor, "Structure-Property Relationships in High Strength Microalloyed Steels," Microalloying 75, Union Carbide Corporation, New York, NY, USA, 32-55.
 11. T. Sakuma and R. W. K. Honeycombe, Met. Sci., 18 (1984), 449-454.
 12. T. Sakuma and R. W. K. Honeycombe, Mater. Sci. Technol., 1 (1985), 351-356.
 13. V. Thillou, M. Hua, C. I. Garcia, C. Perdrix, and A. J. DeArdo, "Precipitation of NbC and Effect of Mn on the Strength Properties of Hot Strip HSLA Low Carbon Steels," Prod. International Conference, "Microalloying in Steels: New Trends for the 21st Century," San Sebastian, 7-9 September, 1998, Editors: J. M. Rodriguez-Ibabe, I. Gutiérrez and B. López, pp. 311-318.
 14. C. Parish, Unpublished Research, BAMPRI, University of Pittsburgh, 2001.
 15. Jinghui Wu, Unpublished Research, BAMPRI, University of Pittsburgh, 2001.
 16. M. Hua, Unpublished Research, BAMPRI, University of Pittsburgh, 2005.
 17. R. G. Smith and R. W. K. Honeycombe, Proc. 6th Int. Conf. on Strength of Metals and Alloys, Melbourne, (1982), 407.
 18. P. L. Mangonon, Jr., and W. E. Heitmann, Microalloying 75, Union Carbide Corporation, New York, NY, 1977, 59-70.
 19. M. I. Santella, "Grain growth and high-temperature hot rolling behavior of low-alloy steel austenite", PhD thesis, University of Pittsburgh, PA, 1981, 49.
 20. T. Parayil and G. Ludkovsky, Proc Accelerated Cooling of Rolled Steel, Pergamon Press, New York, 1988, 131-146.
 21. A. Itman, K. R. Cardoso and H. -J. Kestenbach: Mater. Sci. Technol., 13 (1997), 49-55.
 22. H. Tamehiro, et al., "Application of Accelerated Cooling After Controlled Rolling to Line Pipe Steel," Proc. Third International Conference on Steel Rolling: Technology of Pipe and Tube and Their Application., Iron & Steel Inst. of Japan, 1985, 545-551.
 23. Proc. Accelerated Cooling of Steel, Aug. 19-21, 1985, Pittsburgh, TMS-AIME, 1986.
 24. H. Morikawa and T. Hasegawa, Proc. Accelerated Cooling of Steel, Aug. 19-21, 1985, Pittsburgh, TMS-AIME, (1986), 83-96.
 25. R. G. Davies, "Influence of Martensite Composition and Content on the Properties of Dual Phase Steels," Metall. Trans. A, Vol. 9A, (1978), 671.
 26. S. Okaguchi, T. Hashimoto and H. Ohtani: Proc. Conf. Thermec'88, Vol. 1, 1988, Tokyo, Iron and Steel Institute of Japan, 330-336.
 27. H. Tamehiro, et al, Proc. Accelerated Cooling of Steel, Aug. 19-21, 1985, Pittsburgh, TMS-AIME, 1986., 401-413.
 28. F. B. Pickering: Microalloying '75, Union Carbide Corp., New York, NY (1977), 9.
 29. C.I. Garcia and A.J. DeArdo, "Structure and Properties of ULCB Plate Steels for Heavy Section Applications", Microalloyed HSLA Steels, (ASM International: 1988), 291-300.
 30. H. Ohtani, et al. Metall. Trans. A, Vol. 21A (1990), 877-888.
 31. A. B. Cota and D. B. Santos, Materials Characterization, Vol. 44 (2000), 291-299.
 32. M. Diaz-Fuentes, A. Iza-Mendia, I. Gutierrez, Metall. Mater. Trans. A, Vol.34A (2003), 2505-2516.
 33. M. Takahashi et al., Proc. Intern. Conf. On TRIP-Aided High Strength Ferrous Alloys, Ghent, June 19-21, 2002, 103-111.
 34. H. Matsuda, et al, ibid, 112-119.
 35. Jinghui Wu, Peter J. Wray, Calixto I. Garcia, Mingjian Hua and Anthony J. DeArdo, "Image Quality Analysis: A New Method of Characterizing Microstructure," ISIJ International, Vol. 45 (2005) No. 2, pp254-262.
 36. C. S. Barrett and T. B. Massalski, Structure of Metals, McGraw-Hill, New York, 1966, p. 459.
 37. J. Wu, P. J. Wray, C. I. Garcia, M. Hua, A. J. DeArdo, "On achieving a better understanding of the polygonal ferrite microstructure in if steel using image quality analysis," Materials and Manufacturing Processes, vol. 22, no. 2, February, 2007, p 281-285.
 38. J. Wu, C. I. Garcia, M. Hua, W. Gao, K. Cho, and A. J. DeArdo, "A New Method of Characterizing and Quantifying Complex Microstructures in Steels," Invited Paper, Steel Product Metallurgy and Applications, Organized by B.D. Nelson, and M.J. Merwin, Materials Science and Technology (MS&T) 2006: Product Manufacturing, Materials (ACerS, AIST, ASM, and TMS), pp.305-316.
 39. K. Cho, C. I. Garcia, H. Shu, T. R. Chen and A. J. DeArdo, "Development of the 590 - 780 - 980 Nb-Bearing Dual-Phase Steels for Production on Continuous Galvanizing Lines," Proceedings International Conference on Microalloyed Steels: Processing, Microstructure, Properties and Performance Proceedings, Edited by A. J. DeArdo and C. I. Garcia, July 16-19, 2007, Pittsburgh, PA, AIST, Warrendale, PA, (2007), p313-323.
 40. C. I. Garcia, M. Hua, K. Cho and A. J. DeArdo, "EBSD-IQ: A New Method of Characterizing and Quantifying Complex Microstructures in Steels," Proceedings International Conference on Microalloyed Steels: Processing, Microstructure, Properties and Performance Proceedings, Edited by A. J. DeArdo and C. I. Garcia, July 16-19, 2007, Pittsburgh, PA, AIST, Warrendale, PA, (2007), p335-344.
 41. K. Cho, EBSD Analysis on Bainitic Plate Steel, Unpublished Research, BAMPRI, University of Pittsburgh, 2007.
 42. D.Q. Bai, F. Hamad, J. Asante, and S. Hansen, "Precipitation Strengthening in a Low Carbon Nb- Microalloyed Steel," Materials Science Forum Vols. 500-501 (2005), 481-488
 43. P. E. Repas, "Metallurgical Fundamentals for HSLA Steels," Microalloyed HSLA Steels, ASM International, 1988, 3-14.

Abstract

Rassegna sulla resistenza degli acciai microlegati

Parole chiave: acciaio, lavorazioni plastiche, proprietà

A metà degli anni 1950, gli acciai al carbonio laminati a caldo avevano un alto contenuto di carbonio, microstrutture a grossi grani di ferrite-pearlite, e un limite di snervamento intorno a 300 MPa. La loro duttilità, tenacità e saldabilità erano scarse. Oggi, mezzo secolo più tardi, gli acciai laminati a caldo possono presentarsi con microstrutture costituite da combinazioni di ferrite, bainite e martensite in varie proporzioni. Queste strutture sono molto fini e sono in grado di esibire una resistenza allo snervamento superiore a 900 MPa, con livelli accettabili di duttilità, tenacità e saldabilità. Questo sviluppo è stato reso possibile dalla combinazione dei miglioramenti nella produzione dell'acciaio, nella tecnica di microalligazione e nelle procedure di laminazione e raffreddamento. Lo scopo di questo documento è quello di riportare una cronaca di alcuni dei maggiori progressi nell'alligazione dell'acciaio e nella progettazione dei processi, che hanno portato a questo straordinario risultato.